Article

pubs.acs.org/Biomac

Peptides at the Interface: Self-Assembly of Amphiphilic Designer Peptides and Their Membrane Interaction Propensity

Karin Kornmueller,[†] Bernhard Lehofer,[†] Claudia Meindl,[‡] Eleonore Fröhlich,[‡] Gerd Leitinger,[§] Heinz Amenitsch,[∥] and Ruth Prassl*[,†]

[†]Institute of Biophysics, Medical University of Graz, BioTechMed-Graz, Harrachgasse 21/VI, 8010 Graz, Austria

[‡]Center for Medical Research, Core Facility Imaging, Medical University of Graz, Stiftingtalstraße 24, 8010 Graz, Austria

[§]Institute of Cell Biology, Histology and Embryology, Research Unit Electron Microscopic Techniques, Medical University of Graz, Harrachgasse 21, 8010 Graz, Austria

[∥]Institute of Inorganic Chemistry, Graz University of Technology, Stremayrgasse 9/4, 8010 Graz, Austria

Supporting Information

ABSTRACT: Self-assembling amphiphilic designer peptides have been successfully applied as nanomaterials in biomedical applications. Understanding molecular interactions at the peptide−membrane interface is crucial, since interactions at this site often determine (in)compatibility. The present study aims to elucidate how model membrane systems of different complexity (in particular single-component phospholipid bilayers and lipoproteins) respond to the presence of amphiphilic designer peptides. We focused on two short anionic peptides, V_4WD_2 and A_6YD, which are structurally similar but showed a different self-assembly behavior. A_6YD self-assembled into high aspect ratio nanofibers at low peptide concentrations, as evidenced by synchrotron small-angle X-ray scattering and electron microscopy. These supramolecular assemblies coexisted with membranes without remarkable interference. In contrast, V_4WD_2 formed only loosely associated assemblies over a large concentration regime, and the peptide promoted concentration-dependent disorder on the membrane arrangement. Perturbation effects were observed on both membrane systems although most likely induced by different modes of action. These results suggest that membrane activity critically depends on the peptide's inherent ability to form highly cohesive supramolecular structures.

INTRODUCTION

Molecular self-assembly provides a powerful route to create highly structured materials at the nanoscale. The versatile applicability of these materials—especially in nanomedicine—is equally intriguing as challenging.[1−4] It is indispensable that they are biocompatible, biodegradable, and environmentally safe. One class of molecules has gained recent attention for its high potential as building blocks to design biocompatible supramolecular structures via self-assembly: amphiphilic designer peptides.[5,6] They are exclusively composed of amino acids, are short in sequence (approximately 7−20 residues), and consist of hydrophilic and hydrophobic residues. Due to their amphiphilic nature, they spontaneously self-assemble into highly ordered nanostructures when they exceed a critical aggregation concentration (CAC). Various shapes have been observed, including spherical micelles, tubes, long fibers, or ribbons.[7] Only recently the first supramolecular self-assembled double helix was described.[8] At high peptide concentrations, tight networks of intertwined assemblies form, which often show hydrogel properties.[5,9,10] Up to now, most studies focused on the structural aspects of short amphiphilic designer peptides in solution, but little is known about how biological systems respond to the presence of peptide materials. A recent study addresses this issue for a related class of molecules. For cationic peptide amphiphiles (PAs, consisting of a peptide sequence covalently attached to an alkyl tail[11]), it was demonstrated that the strength of supramolecular cohesion within self-assembled materials had a crucial impact on whether cells are viable in the PA's vicinity.[12] We followed on this highly interesting approach with the aim to find out if the same principles apply for short amphiphilic designer peptides and to shed light on features that determine peptide−membrane compatibility. Before progressing to cellular systems, model membrane systems, such as phosphatidylcholine multilamellar vesicles (MLVs) and low density lipoproteins (LDL), are a valuable tool in obtaining detailed information on interactions at the peptide−membrane interface. MLVs are composed of well-defined lipid bilayers. They are easy to produce, highly homogeneous, and extremely well characterized. By using LDL, we have applied a model system that has physiological relevance and mimics the

Received: July 19, 2016
Revised: October 13, 2016

DOI: 10.1021/acs.biomac.6b01089
Biomacromolecules XXXX, XXX, XXX−XXX

molecular heterogeneity of a cell membrane, as it contains protein, different phospholipid species,[13] cholesterol,[14] and glycosylated structures. These characteristics are combined with the opportunity to target peptide interactions to one of LDL's compartments: the hydrophobic core or the amphiphilic phospholipid−protein surface monolayer. Moreover, the LDL particle's composition, its molecular organization,[15] and its thermal transitions[16] are well-defined, making it an ideal system to study peptide−membrane interactions.

We focus our studies on anionic peptides, which in contrast to their cationic counterparts often receive less attention. However, especially for peptide−material applications, they have the same potential and should thus receive equal consideration. We have chosen A_6YD and V_4WD_2 as two representatives. Both share structural and chemical similarities: they are amphiphilic and have a length of approximately 2.6−3 nm. A_6YD is a derivative of one of the first and best characterized short amphiphilic designer peptides, A_6D.[7,17−21] Its six hydrophobic alanine residues are complemented with a tyrosine spacer residue, followed by a negatively charged aspartic acid, which provides the hydrophilic headgroup. The second peptide (V_4WD_2) was designed to be considerably more hydrophobic due to the presence of four valine residues. In order to compensate for this higher hydrophobicity, and to maintain solubility, two negatively charged aspartic acid residues are incorporated, together with a tryptophan residue, which has a known propensity to intercalate into lipid−water interfaces.[22] Both peptides are acetylated at their N-terminus and have a free carboxyl group at the C-terminus. Thus, V_4WD_2 yields a total of three negative charges, and A_6YD yields a total of two negative charges per molecule at neutral pH. Parts A and B of Figure 1 respectively show the atomic structures of A_6YD and V_4WD_2. Table 1 compares the physicochemical characteristics of both peptides.

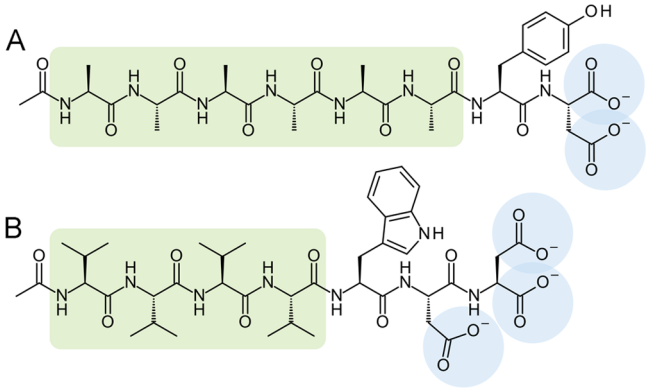

Figure 1. Amino acid sequences of the peptides A_6YD (A) and V_4WD_2 (B). The peptides are acetylated at their N-terminus and have a free carboxyl group at the C-terminus. Highlighted domains represent the hydrophobic parts of the structure (green), as well as charged residues (blue).

Our experimental setup allowed us to study the concentration-dependent evolution of the structure and morphology of peptides from monomers to loosely assembled aggregates or highly ordered self-assembled superstructures. To address the question of how artificial and biological membranes adapt when in contact with peptides, we monitored structural and dynamic alterations by a combination of various biophysical techniques, namely, differential scanning calorimetry (DSC), electron paramagnetic resonance (EPR) spectroscopy, small-angle X-ray scattering (SAXS), and transmission electron microscopy (TEM).

We could demonstrate that intermolecular cohesion is linked to the evolution of stable supramolecular structures and is thus the prerequisite that peptide assemblies coexist with membranes: the peptide A_6YD forms long, fibrous supramolecular assemblies above its CAC and shows only a weak propensity to interact with membranes. In contrast, V_4WD_2 does not assemble into ordered supramolecular architectures over a large concentration regime and the peptide induces a concentration-dependent destabilization effect on synthetic as well as biological membranes.

EXPERIMENTAL SECTION

Chemicals. The peptides ac-A_6YD (A_6YD), ac-V_4WD_2 (V_4WD_2), and ac-A_6YK-NH_2 (A_6YK) were custom synthesized and purified by piCHEM GmbH (Graz, Austria) and Peptide 2.0 (Chantilly, VA, USA). High-performance liquid chromatography (HPCL) and mass spectrometry (MS) data of the peptides are provided in the Supporting Information (Figures S1−S6). Dipalmitoylphosphatidylcholine (DPPC) was purchased from Avanti Polar Lipids (Alabaster, AL, USA). 1,6-Diphenyl-1,3,5-hexatriene (DPH) and the spin labels 5-doxyl-stearic acid (5-DSA) and 7-doxyl-stearic acid methyl ester (7-MeDSA) were purchased from Sigma-Aldrich (Vienna, Austria). CPD-buffered (anticoagulant citrate phosphate dextrose solution) plasma was obtained from the Department of Blood Group Serology and Transfusion Medicine (Medical University of Graz, Austria). Blood was sampled from healthy subjects after obtaining written informed consent, according to a protocol approved by the Institutional Review Board of the Medical University of Graz. All other chemicals were purchased either from Sigma-Aldrich (Vienna, Austria), Carl Roth GmbH (Karlsruhe, Germany), or SERVA Electrophoresis GmbH (Heidelberg, Germany) and were of analytical grade.

Investigating Peptide Supramolecular Structure Formation. *Peptide Preparation.* Lyophilized peptides were dissolved in double-distilled water. NaOH (1 or 0.1 M) was added stepwise until the samples appeared as clear, colorless solutions. Stock solutions (50 mM) were then diluted with double-distilled water to obtain the desired concentrations. All samples were aged for 1 week under an argon atmosphere prior to fluorescence, SAXS, TEM, and attenuated total reflection Fourier transform infrared (ATR-FTIR) spectroscopy measurements.

Determination of the Critical Aggregation Concentration (CAC). A 4 μL portion of DPH in methanol (10 μM) was added to 50 μL of peptide solution of varying concentrations. All fluorescence spectra were recorded under identical conditions on a CLARIOstar microplate reader (BMG LABTECH, Ortenberg, Germany) with an excitation wavelength of 359 nm. Fluorescence emission was recorded at 428 nm. Samples were background corrected and normalized to the highest intensity readout. DPH is almost nonfluorescent in aqueous solutions and in the presence of randomly oriented peptide monomers. As soon as oriented structures are formed, a sharp increase in fluorescence intensity is observed. The CAC of the peptide is defined as the

Table 1. Physicochemical Characteristics of A_6YD and V_4WD_2

peptide	no. of amino acids	net charge at pH 7	MW (g/mol)	hydrophobicity (GRAVY)[23]	~CAC (mM)	aromatic amino acid
A_6YD	8	−2	765	0.75	3	Tyr
V_4WD_2	7	−3	873	1.27	>7.5	Trp

DOI: 10.1021/acs.biomac.6b01089
Biomacromolecules XXXX, XXX, XXX−XXX

intersection point of two straight lines, fitting the low intensity region and the region with linearly increasing intensity.[18]

Small Angle X-ray Scattering (SAXS). Supramolecular structure formation was investigated on a concentration series, covering 1−50 mM for V_4WD_2 and 0.25−40 mM for A_6YD. Synchrotron X-ray scattering data was collected at the Austrian SAXS beamline at ELETTRA (Trieste, Italy).[24] Measurements were conducted at a wavelength of 0.154 nm and a sample−detector distance of 1.1 m. The photon energy was 8 keV. The X-ray images were recorded with a Pilatus detector (PILATUS 100K or Pilatus3 1M, DECTRIS Ltd., Villigen PSI, Switzerland), calibrated with silver behenate. The scattering intensity was measured as a function of the scattering vector q where

$$q = 4\pi(\sin\theta)/\lambda$$

with 2θ being the scattering angle and λ being the wavelength. Samples were measured in a 1.5 mm glass capillary. Data analysis was done with Fit2D[25] and Igor Pro (Version 6.22A, WaveMetrics Inc., USA). Experimental intensities were corrected for fluctuation of the primary intensity, transmission, and background.

Negative Staining Transmission Electron Microscopy (TEM). Solutions of A_6YD and V_4WD_2 (11 mM) were incubated for 1 week prior to TEM measurements. Samples were adsorbed onto a glow-discharged carbon-coated copper grid and allowed to settle for 1 min. Excess fluid was carefully removed with filter paper and immediately replaced by 5 μL of a 2% (w/v) uranyl acetate staining solution, which was centrifuged for 6 min at 10000 rpm prior to usage in order to precipitate potentially present aggregates. The uranyl acetate solution was allowed to settle for 30 s, blotted, and replaced by another 5 μL of fresh solution. After 30 s of incubation, the staining solution was removed and the sample was air-dried. Visualization of the samples was achieved by using a Fei Tecnai G^2 20 transmission electron microscope (Eindhoven, The Netherlands) operating at an acceleration voltage of 120 kV. Digital images were made using a Gatan US1000 CCD camera at 2K × 2K resolution.

Attenuated Total Reflection Fourier Transform Infrared (ATR-FTIR) Spectroscopy. Infrared spectra were recorded on a Bruker ALPHA-T FTIR spectrometer, equipped with an ATR accessory (Bruker Optics Inc., Billerica, USA) between 4000 and 600 cm^{-1}. The spectra were the averages of 128 scans with a resolution of 4 cm^{-1}. Spectra were water corrected, and data analysis was done with OPUS (Bruker Optics Inc., Billerica, USA) and Igor Pro (Version 6.22A, WaveMetrics Inc., USA).

Investigating Peptide−Membrane Interactions on Dipalmitoyl-Phosphatidylcholine Multilamella Vesicles (DPPC MLVs). *Preparation of DPPC MLVs.* DPPC was dissolved in chloroform/methanol (2:1 v/v), mixed, and organic solvents were evaporated under a gentle stream of nitrogen, followed by drying under a vacuum overnight in order to completely remove residual organic solvents. The dry lipid-film was hydrated either by adding double-distilled water (reference) or by adding aqueous solutions of the peptides to finally obtain four different molar ratios: 50:1, 25:1, 10:1, and 5:1 DPPC/peptide (mol/mol). These ratios correspond to peptide concentrations of 1.1, 2.2, 5.5, and 11 mM, respectively. The DPPC concentration was 55 mM. The samples were incubated above the lipid's phase transition temperature at 50 °C for 2 h, intermitted by vigorous vortexing every 15 min.

Differential Scanning Calorimetry (DSC) on DPPC MLVs. DPPC MLVs in the presence and absence of peptides were prepared as described above, incubated for 24 h at room temperature (gently rotating), and diluted with double-distilled water to 2.75 mM DPPC prior to measurements to fit the optimal concentration regime for DSC. Measurements were performed on a Microcal VP-DSC differential scanning calorimeter (Northampton, MA, USA). Scans were recorded at a constant scan rate of 0.5 °C/min from 10 to 80 °C. Each DSC experiment consisted of three heating and three cooling scans. Samples were tempered for 30 min before each heating scan and 10 min before each cooling scan. MicroCal Origin software was used for data acquisition, baseline adjustment, normalization to the phospholipid concentration, and data analysis throughout. The phase transition temperature (T_m) was defined as the temperature at the peak maximum of the heat capacity (c_p). The sharpness of the transition was described by the full width at half-maximum ($\Delta T_{1/2}$), and calorimetric enthalpies (ΔH) were calculated by integrating the peak areas.

Electron Paramagnetic Resonance (EPR) Spectroscopy on DPPC MLVs. Samples were prepared as described above with the exception that the lipid-film was enriched with a spin label in a 100:1 (lipid:spin label) molar ratio. Two different spin labels were used: 5-doxyl-stearic acid (5-DSA) to probe membrane fluidity close to the lipid headgroup region and 7-doxyl-stearic acid methyl ester (7-MeDSA), which goes deeper into the inner hydrophobic part of the bilayers. Samples were incubated for 24 h at room temperature, gently rotating.

EPR spectra were recorded on a Bruker X-band ECS106 spectrometer (Rheinstetten, Germany) at 9.52 GHz. Measurement conditions were as follows: modulation frequency, 50 kHz; scan width, 200 G; modulation amplitude, 2 G; microwave power, 5 mW. Measurements were carried out at 25 and 50 °C. The spectral parameters were determined using the WinEPR software. Spectra typical for rapid anisotropic spin label motions were interpreted as described in the literature[26] with the order parameter S

$$S = \left(\frac{T_{\parallel}' - T_{\perp}'}{T_{zz} - T_{xx}}\right)\left(\frac{a}{a'}\right)$$

The hyperfine tensors $T_{\parallel}'$ and $T_{\perp}'$ were derived from measuring the separation of the outer and inner hyperfine extrema. The isotropic splitting constant a' was determined by the relationship $a' = {}^1/_3(T_{\parallel}' + 2T_{\perp}')$.[27] The parameters a = 14.1 G, $T_{xx} = T_{yy}$ = 5.8 G, and T_{zz} = 30.8 G were derived from the literature.[28] For spectra typical for isotropic motion, the rotational correlation time τ_c was calculated[29,30] with

$$\tau_c = (6.5 \times 10^{-10}) W_0 \left(\sqrt{\frac{h_0}{h_{-1}}} - 1\right)$$

W_0 is the midfield line width, and h_0 and h_{-1} are the heights of the mid- and high-field lines, respectively.

Small Angle X-ray Scattering (SAXS) on DPPC MLVs. DPPC MLVs in the presence of peptides were prepared as described above. Samples were incubated for 24 h at room temperature, gently rotating. Synchrotron SAXS measurements were performed as described above and recorded at 25 °C (below the lipid's phase transition temperature).

Investigating Peptide−Membrane Interactions on Low Density Lipoprotein (LDL). *Isolation and Chemical Characterization of LDL.* LDL was obtained from human plasma by ultracentrifugation at its own density followed by two steps of ultracentrifugation at a density of 1.063 g/cm^3 as described previously.[31] Each centrifugation step was performed in a Sorvall Ultra Pro 80 ultracentrifuge (Newtown, USA) with a Sorvall T-865 fixed angle titanium rotor (DuPont Instruments, Newtown, USA) at 4 °C for 24 h at 50000 rpm. Isolated LDL was extensively dialyzed against 10 mM sodium phosphate buffer (pH 7.4) and concentrated with Amicon Ultra-15 centrifugal filter units (MWCO 100 kDa, Millipore, Billerica, MA).

The chemical composition of LDL was determined by commercially available enzymatic assays: the protein content was measured by the BCA method (BCA Protein Assay, Thermo Scientific, Rockford, USA); phospholipid, triacylglycerol, free, and total cholesterol concentrations were determined with the kits "Phospholipid FS", "Triglycerides FS", "Free Cholesterol FS", and "Cholesterol FS" by DiaSys (DiaSys Diagnostic Systems GmbH, Holzheim, Germany), respectively.

Differential Scanning Calorimetry (DSC) on LDL. LDL ($c_{protein}$ = 5 mg/mL) was incubated with four different peptide concentrations (11, 5.5, 2.2, and 1.1 mM) for 24 h at 4 °C, gently shaking. Samples were diluted 1:3 prior to measurements to fit the optimal concentration regime for DSC. Measurements were carried out as described for DPPC MLVs (see above), except for a scan rate of 1 °C/min and a temperature range from 5 to 95 °C. Calorimetric enthalpies were

DOI: 10.1021/acs.biomac.6b01089
Biomacromolecules XXXX, XXX, XXX−XXX

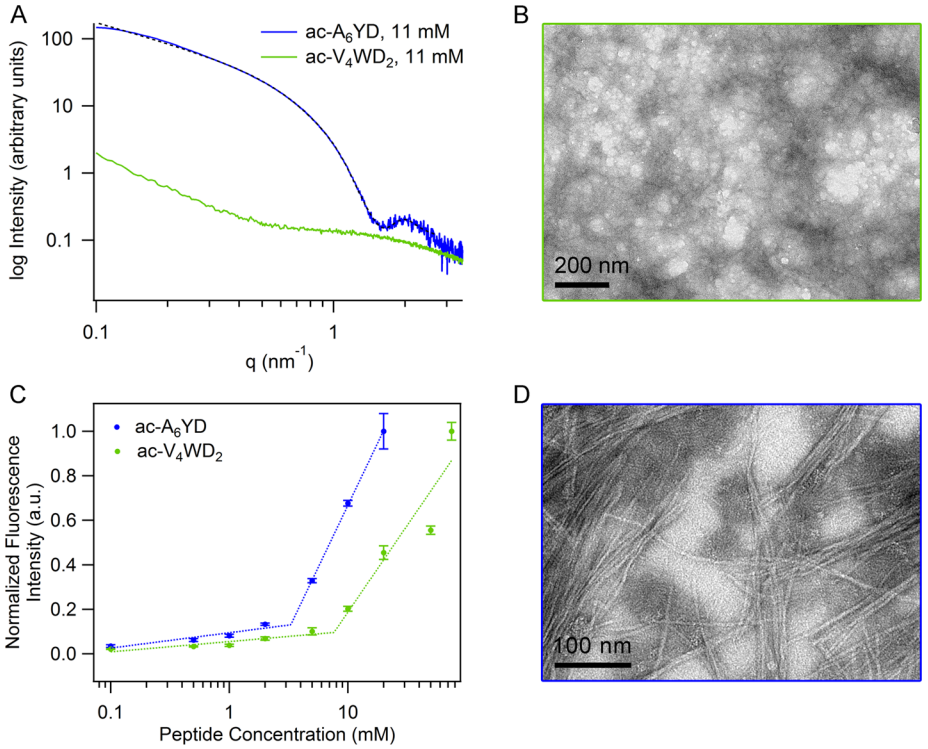

Figure 2. Self-assembly of the peptides A_6YD and V_4WD_2. Experimental scattering patterns of A_6YD (A, blue curve) and V_4WD_2 (A, green curve) at a concentration of 11 mM show that only A_6YD formed defined supramolecular structures. The SAXS pattern could be fitted with a core−shell cylinder form factor model (dashed black curve). Also, TEM micrographs (D) confirm the presence of extended fibrous structures. Neither SAXS (A, green curve) nor TEM (B) detected ordered supramolecular assemblies for 11 mM V_4WD_2. The rise in intensity at low q-values of the V_4WD_2 scattering pattern characterized the onset of peptide aggregation. TEM micrographs show that the sample consists of mostly unstructured aggregates (B). With fluorescence depolarization, these aggregates are already detected and therefore a CAC of around ∼7.5 mM (C, green fit) is determined. A_6YD shows a CAC of ∼3 mM (C, blue fit).

calculated by integrating the peak areas after baseline adjustment and normalization to either cholesterylester or protein content.

Electron Paramagnetic Resonance (EPR) Spectroscopy on LDL. The spin labels 5-DSA and 7-MeDSA were dissolved in ethanol and dried under a stream of nitrogen. The appropriate amounts of spin label depended on LDL composition. The amount of 5-DSA was related to the phospholipid content (∼13 mM), whereas 7-MeDSA was related to the amount of core lipids (∼45 mM, cholesterylesters and triacylglycerol). The final lipid:spin label ratio was adjusted to 100:1 (mol/mol). The dry film was dispersed in lipoprotein solution and incubated under an argon atmosphere for at least 2 h at 4 °C on a shaker to allow the spin label to incorporate into the LDL particle. Aqueous solutions of the peptides were added to the spin labeled LDL preparations to obtain different ratios—50:1, 25:1, and 10:1 phospholipid/peptide (mol/mol)—followed by incubation for 24 h at 4 °C. Samples were investigated at 10, 25, and 37 °C. The measurement parameters were identical to those for DPPC MLVs (see above: EPR spectroscopy on DPPC MLVs).

Small Angle X-ray Scattering (SAXS) on LDL. LDL ($c_{protein}$ = 5 mg/mL) was incubated with four different peptide concentrations (final concentrations: 11, 5.5, 2.2, and 1.1 mM) for 24 h at 4 °C, gently shaking. Synchrotron SAXS measurements were performed as described above.

Negative Staining Transmission Electron Microscopy (TEM) on LDL. LDL ($c_{protein}$ = 5 mg/mL) was incubated with the highest peptide concentration (11 mM) of A_6YD and V_4WD_2 for 24 h at 4 °C, gently shaking. Serial dilutions of the samples were prepared directly before negative staining to obtain the optimum concentration for imaging (1:10 dilution). Negative staining and TEM were conducted as described above.

RESULTS AND DISCUSSION

Supramolecular Structure Formation. To study the self-assembling properties of A_6YD and V_4WD_2, we used the complementary characterization techniques synchrotron SAXS, ATR-FTIR, and negative-staining TEM. Concentration-dependent SAXS measurements of V_4WD_2 suggest a rather slow start of aggregation. Over a large concentration regime (1 to ∼50 mM), no defined superstructures are present (Figure S7A). One example is shown in Figure 2A: 11 mM V_4WD_2 lacks complex assemblies, but a slow rise in intensity at low q values indicates the onset of peptide aggregation (Figure 2A, lower green SAXS pattern). Also, TEM images show only inhomogeneously distributed dense aggregates for this concentration (Figure 2B). ATR-FTIR measurements reveal that already at low peptide concentrations elements of secondary structure are present. Spectrograms show a concentration-dependent signal development in the amide I region at 1630 nm^{-1}, which is indicative of β-type structures (Figure S7B). We assume that almost immediately peptide monomers assemble into small oligomeric aggregates, most probably due to hydrogen bonding interactions between valine residues. This behavior causes the rise in intensity in the SAXS pattern and results in a characteristic β-sheet IR pattern. Therefore, the experimentally determined CAC value of ∼7.5 mM can only be seen as a rough estimate (Figure 2C). The method of fluorescence depolarization[18] detects also signals from small aggregates, but it does not tell anything about the quality or complexity of a structure. Our results suggest that

DOI: 10.1021/acs.biomac.6b01089
Biomacromolecules XXXX, XXX, XXX−XXX

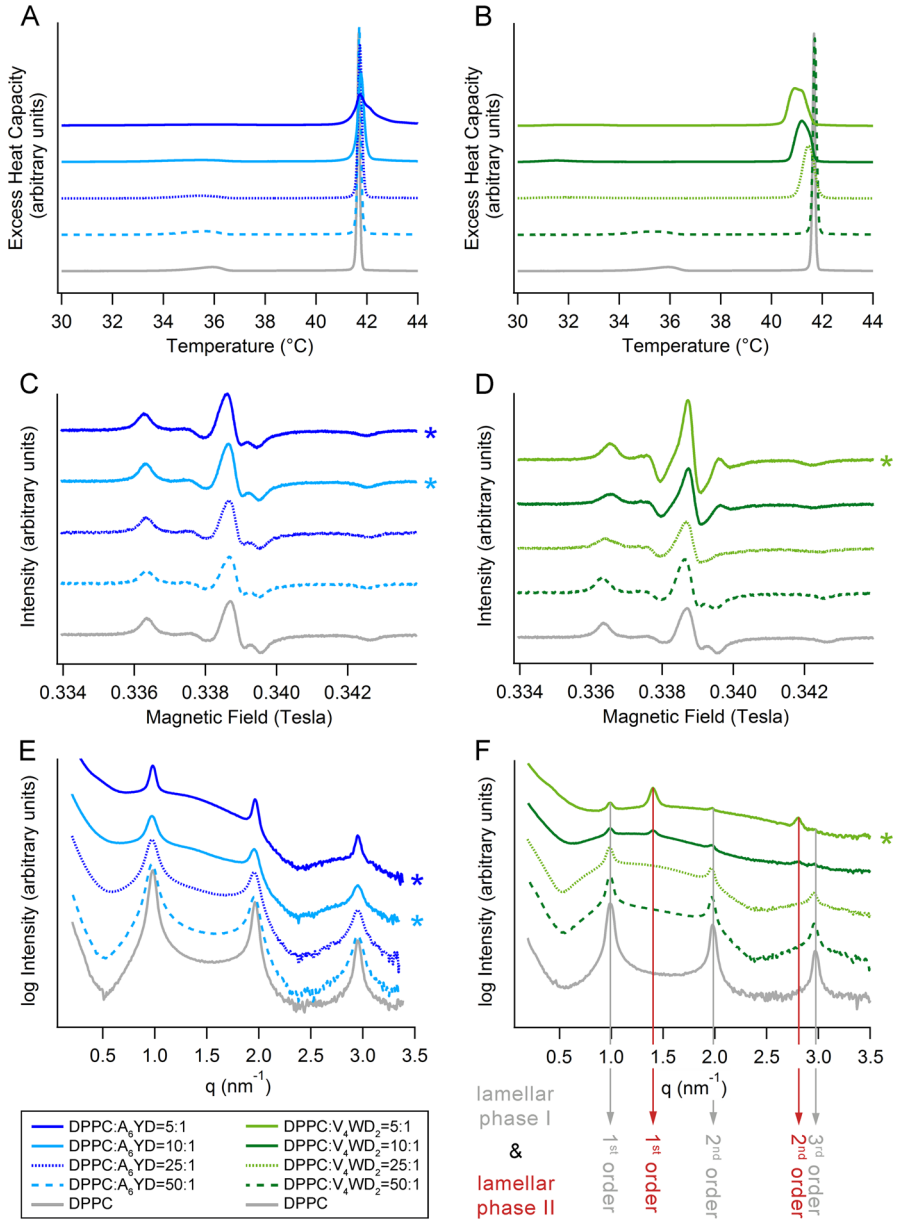

Figure 3. Biophysical characterization of DPPC−peptide interactions by DSC (A/B), EPR spectroscopy (C/D), and SAXS (E/F). DSC thermograms show the DPPC heat capacity c_p as a function of temperature in the presence of A_6YD (A) and V_4WD_2 (B). Pure DPPC MLVs (gray curves) show two characteristic transitions, one at ∼36 °C (pretransition) and another at 41.7 °C (main-transition). Both peptides caused a concentration-dependent disappearance of the pretransition. A_6YD led to an increase in $\Delta T_{1/2}$ only at its highest concentration, whereas V_4WD_2 induced a concentration-dependent broadening of the main-transition peak, as well as a temperature shift. EPR spectra at 25 °C with a 5-DSA spin label are typical for anisotropic motions in membranes (C/D). A_6YD has no effect on spin label mobility (C). In contrast, V_4WD_2 led to a concentration-dependent decrease in the order parameter (D). SAXS patterns of pure DPPC (gray curve) at 25 °C show three reflection orders, which are maintained in the presence of A_6YD (E) but rearranged in combination with the emergence of a second lamellar phase in the presence of V_4WD_2 (F). All spectra were shifted in the *y*-axes for clearer visibility. The asterisks mark samples where the peptide concentration lies above the CAC at measurement conditions.

below ∼50 mM V_4WD_2 peptides are present only as loosely connected aggregates, without microscopic order.

In contrast, A_6YD assembly starts around 3 mM (Figure 2C), and its scattering patterns show a concentration-dependent development into cylindrical structures (Figure S7C and Figure 2A, blue curve). Scattering in the low *q*-range showed a q^{-1} dependence, and indeed, the best fit was obtained with a hollow cylinder form factor model.[32] The assemblies were characterized by a cross-sectional radius of ∼3.3 nm and a shell thickness of ∼1.7 nm. All additional fitting parameters are listed in Table S1 in the Supporting Information. SAXS data were in good agreement with TEM images. Micrographs (Figure 2D) showed a dense network of high aspect ratio nanofibers, with lengths extending to several hundreds of nanometers, whereas their diameters were only around 6−10 nm and appeared fairly uniform. Accordingly, A_6YD and V_4WD_2 show a completely different self-assembly behavior.

Self-assembly and the resultant morphologies of the superstructures are driven by a finely balanced interplay between the hydrophobic interactions of tail residues, electro-

DOI: 10.1021/acs.biomac.6b01089
Biomacromolecules XXXX, XXX, XXX−XXX

static interactions between charged headgroups, chiral dipole−dipole interactions, $\pi-\pi$ stacking of aromatic residues, intermolecular hydrogen bonds, nonspecific van der Waals interactions, and repulsion due to steric hindrances. Even more complexity is added due to the influence of environmental conditions (such as solvent polarity, pH, temperature, incubation time, etc.). This plethora of variables makes it almost impossible to derive general rules for peptide assembly. We kept the environmental conditions for our samples as constant as possible; nevertheless, it has to be mentioned that our results can only present a snapshot for exactly these two peptides under the investigated conditions. Therefore, what determines the difference between A_6YD and V_4WD_2 assembly? We assume that electrostatic repulsion due to three negative charges within V_4WD_2 is so dominant that it limits intermolecular attractive forces (including the high propensity of valines to form hydrogen bonds, or $\pi-\pi$ stacking of tryptophan residues). Thus, self-assembly into macroscopically ordered structures is impeded and V_4WD_2 samples contain rather loosely connected aggregates. A_6YD has only two negative charges in total, combined with a considerably longer hydrophobic tail of six alanine residues. In this arrangement, the hydrophobic attraction between tail residues outbalances electrostatic repulsion of the charged head and self-assembly is possible.

Knowing these characteristics in the self-assembling behavior, in the next step, we aimed to monitor if these differences translate to a different impact on membrane interfaces. We distinguish between (1) peptides at low concentrations (present in a dispersed state in the form of monomers, loose aggregates, or small oligomers), (2) loosely assembled aggregates at high peptide concentrations (V_4WD_2), and (3) highly ordered peptide superstructures (A_6YD above its CAC).

Interfacing Peptides with a Synthetic Membrane Mimic. DPPC MLVs are a single-component lipid system and are mimicking membrane-bilayer structures in a very basic way.[33] Studying the thermotropic phase behavior of fully hydrated DPPC MLVs in the presence and absence of peptides by DSC is one of the most sensitive and easiest means to investigate the peptide's effect on membrane mimics. Thermograms of DPPC in the presence of low A_6YD concentrations showed the same characteristics as pure DPPC MLVs. They exhibited a pretransition (T_{pre}) from the lamellar gel (L_{β}') to the rippled gel phase (P_{β}') at around 35.5 °C and a main-transition (T_m) at 41.7 °C to the liquid crystalline (L_{α}) phase. The DPPC main-transition displayed an extremely narrow half-width of $\Delta T_{1/2}$ = 0.11, indicative for highly cooperative chain melting. With increasing A_6YD concentrations, this cooperativity was slightly reduced, indicated by a gentle broadening of the main-transition peak. At the same time, the enthalpy (ΔH) slightly increased, pointing toward a stabilizing effect. Only the highest A_6YD concentration led to typical signs of membrane destabilization: a loss of the pretransition peak, a considerable broadening of the main-transition peak, with $\Delta T_{1/2}$ = 0.67, in combination with a slightly reduced ΔH value (see Figure 3A and Table 2). The destabilizing effect was much more pronounced in the case of V_4WD_2 (see Figure 3B and Table 3). Even low peptide concentrations led to peak-broadening and temperature shifts in both transitions. These effects became more pronounced with increasing peptide concentrations. The highest V_4WD_2 peptide concentration (5:1 molar ratio) showed a decrease in T_m from 41.7 °C (pure DPPC) to 40.9 °C and an increase in $\Delta T_{1/2}$ from 0.11 to 0.79, paired with the emergence of a second shoulder, which marked a considerable extent of perturbation in the membrane.

Table 2. DSC Parameters of Pure DPPC and DPPC−A_6YD Mixtures of Varying Lipid:Peptide Molar Ratios

sample	T_{pre} (°C)	T_m (°C)	$\Delta T_{1/2}$	ΔH (kcal/mol/°C)
DPPC	35.9	41.7	0.11	10.0
DPPC:A_6YD = 50:1	35.7	41.7	0.13	12.1
DPPC:A_6YD = 25:1	35.5	41.7	0.17	11.8
DPPC:A_6YD = 10:1	35.5	41.8	0.26	12.1
DPPC:A_6YD = 5:1	n.d.[a]	41.7	0.67	10.5

[a]n.d., not detectable.

Table 3. DSC Parameters of Pure DPPC and DPPC−V_4WD_2 Mixtures of Varying Lipid:Peptide Molar Ratios

sample	T_{pre} (°C)	T_m (°C)	$\Delta T_{1/2}$	ΔH (kcal/mol/°C)
DPPC	35.9	41.7	0.11	10.0
DPPC:V_4WD_2 = 50:1	35.4	41.7	0.16	10.5
DPPC:V_4WD_2 = 25:1	32.0	41.5	0.54	10.2
DPPC:V_4WD_2 = 10:1	31.5	41.2	0.69	9.1
DPPC:V_4WD_2 = 5:1	32.9	40.9	0.79	10.3

These results gave a first indication that A_6YD and V_4WD_2 interact differently with lipid membranes. They prompted us to look deeper into the mode of action of both peptides. To target the peptides' sites of action, we applied EPR spectroscopy, which allows investigating the conformational dynamics in local microenvironments within a membrane. Due to their structural analogy to membrane lipids, we used the doxyl-stearic acid spin labels 5-DSA and 7-MeDSA. Both spin labels incorporate into the bilayer but partition into different depths.[26] In 5-DSA, the paramagnetic doxyl group is attached to the C_5-position of the hydrocarbon chain, and situates the spin probe close to the bilayer interface region. 7-MeDSA has a doxyl group at the C_7-position, and is considerably more lipophilic due to its electrically neutral methyl group, and therefore is used to probe lipid chain fluidity in deeper and more hydrophobic regions of the bilayer. All obtained spectra showed typical characteristics of highly anisotropic motion (Figure S8, Tables S2 and S3). In pure DPPC MLVs, lipid mobility is restricted in the polar headgroup region (reflected by a high order parameter, $S_{5\text{-DSA}}$ = 0.99 at 25 °C), whereas the hydrocarbon chain region allowed higher rotational flexibility ($S_{7\text{-MeDSA}}$ = 0.72 at 25 °C). The addition of A_6YD yielded very similar results (Figure 3C, Table S2), and thus, we conclude that the peptide had no impact on membrane dynamics, regardless of peptide concentration, spin label, or temperature (measured below (25 °C) and above (50 °C) the lipid phase transition). In contrast, V_4WD_2 led to an increase in DPPC lipid motion (Figure 3D, Table S2). However, this effect was only limited to the surface region, as indicated by changes in S in the presence of 5-DSA but not 7-MeDSA. With increasing V_4WD_2 concentrations, the order parameter drops to about 75% of its original value (from $S_{5\text{-DSA}}$ = 0.99 to 0.75 at 25 °C). This implies that the peptide loosened the tight packing of the phospholipid headgroups. At the same time, the hyperfine splitting increased from $a_{5\text{-DSA}}'$ = 14.4 for pure DPPC to a maximum of $a_{5\text{-DSA}}'$ = 15.3 in the presence of V_4WD_2 (Table S3). This indicates a higher polarity in the spin label's microenvironment, likely due to an intercalation of the attached peptide molecules.

DOI: 10.1021/acs.biomac.6b01089
Biomacromolecules XXXX, XXX, XXX−XXX

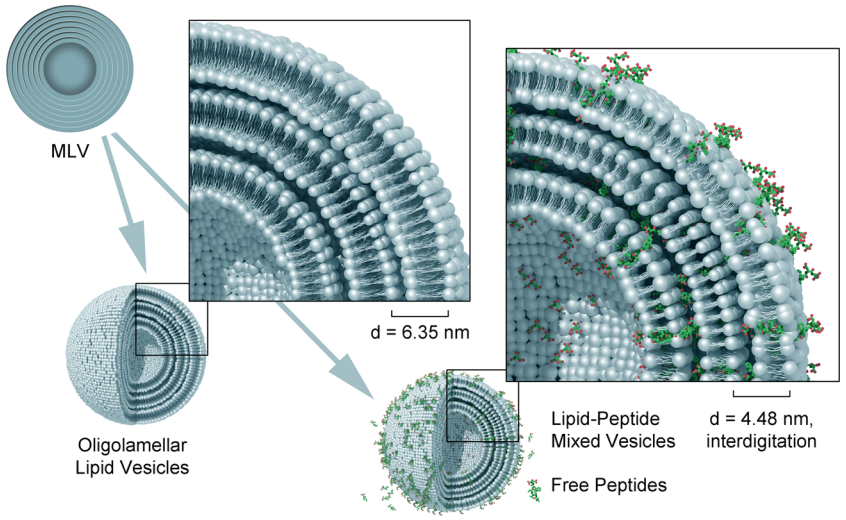

Figure 4. In contrast to pure DPPC MLVs, the presence of V_4WD_2 induced the formation of two different vesicle populations within the sample: DPPC oligolamellar vesicles and lipid−peptide mixed vesicles. Oligolamellar vesicles showed a reduced number of layers but the same *d*-spacing as DPPC MLVs (6.35 nm). At the same time, lipid−peptide mixed vesicles formed, also with a lamellar internal arrangement. Their *d*-spacing was only 4.48 nm, most likely due to peptide-induced interdigitation of phospholipid acyl chains.

To study global structural changes, we used synchrotron SAXS. In the presence of low peptide concentrations, we found that the scattering pattern maintains the major characteristics of pure DPPC, displaying three reflection orders with sharp equidistant peaks and an associated lamellar spacing of d = 6.41 nm.[33] The closer the CAC is approached, the higher the contribution of diffuse scattering, paired with a decrease in Bragg peak intensity. This effect might be attributed to a peptide-induced conversion of MLVs to oligolamellar vesicles with positionally less or noncorrelated bilayers. At higher peptide concentrations, this scattering contribution remains as a constant fraction (corresponding to the maximum amount of monomers in the bulk phase, at the CAC). As soon as supramolecular structures or larger peptide aggregates are formed, the changes in the scattering patterns are peptide-dependent. Changes induced by A_6YD superstructures are subtle, and the global morphology of the DPPC scattering pattern is maintained (Figure 3E). What adds is the scattering contribution of the assembled peptide cylinders. In contrast, the addition of only loosely packed V_4WD_2 aggregates induced a considerable reorganization of MLVs (Figure 3F). Via an intermediate state of uncorrelated bilayered stacks (Figure 3F, DPPC:V_4WD_2 = 25:1), the peptide gave rise to the formation of a new lamellar phase with a much smaller *d*-spacing of d = 4.48 nm (Figure 3F, red arrows). This second lamellar phase was favored by increasing peptide concentrations—at the expense of the pure DPPC peaks with d = 6.35 nm (Figure 3F, gray arrows). The huge difference in the lamellar *d*-spacing (about 1.87 nm) makes a coexistence of domains (peptide rich/peptide poor) associated with membrane thinning within a single particle very unlikely. Instead, the data provide evidence that these two lamellar phases exist as two separate particle populations within the sample. As shown in Figure 4, one could expect that, depending on the peptide concentration, oligolamellar lipid vesicles with a reduced number of bilayers are formed instead of MLVs. In coexistence, peptide−lipid mixed vesicles are formed, which were also lamellar in structure but showed a much smaller *d*-spacing likely due to interdigitation of phospholipid acyl chains.

Combining the information obtained from CAC determination, SAXS, DSC, and EPR studies, we have seen that A_6YD and V_4WD_2 have different self-assembling propensities, which result in different membrane-activity profiles. V_4WD_2 peptide assemblies are structurally less defined and their formation starts only at high peptide concentrations, limited most likely due to self-repulsion of negatively charged aspartic acid residues. However, we presume that it is the negative charges which attract peptides to the zwitterionic DPPC membranes. Tryptophan's inherent propensity to intercalate and cluster near membrane−water interfacial regions and the high hydrophobicity of valine residues favor insertion into the headgroup region of the bilayer, thus resulting in membrane destabilization. In contrast, A_6YD almost immediately assembles into long hollow cylindrical nanofibers. DSC results show that an A_6YD concentration close to the CAC results in weak membrane destabilization, whereas at concentrations above the CAC the peptide shows almost no tendency to interact with DPPC MLVs. The concept of dissolution reassembly between peptide superstructures and monomers in equilibrium is widely used to describe the dynamic nature of peptide assembly. We suggest that, as soon as the CAC is exceeded, peptides show a higher affinity to take part in the exchange between bulk phase and assemblies than being directed toward DPPC.

To support this notion, we next investigated the positively charged analogue of A_6YD, namely, A_6YK (Figure S9) which has an even lower CAC (~1 mM, Figure S10). The peptide self-assembled into extended cylinders that looked similar to A_6YD's supramolecular structures, although the networks appeared even tighter (Figure S11). During the sample preparation procedure of negative-staining TEM, the sample solution is blotted several times and left to dry on the grid. Especially for peptide samples, this can cause problems, because supramolecular structure development is often concentration-dependent, and evaporation and blotting might lead to the formation of artifacts. We therefore investigated the same sample also under cryogenic conditions, which are known to be less invasive. A direct comparison between negative-staining and cryo-TEM yielded similar results, and a similar quality of microscopic images. Visualized by both techniques, A_6YK

DOI: 10.1021/acs.biomac.6b01089
Biomacromolecules XXXX, XXX, XXX−XXX

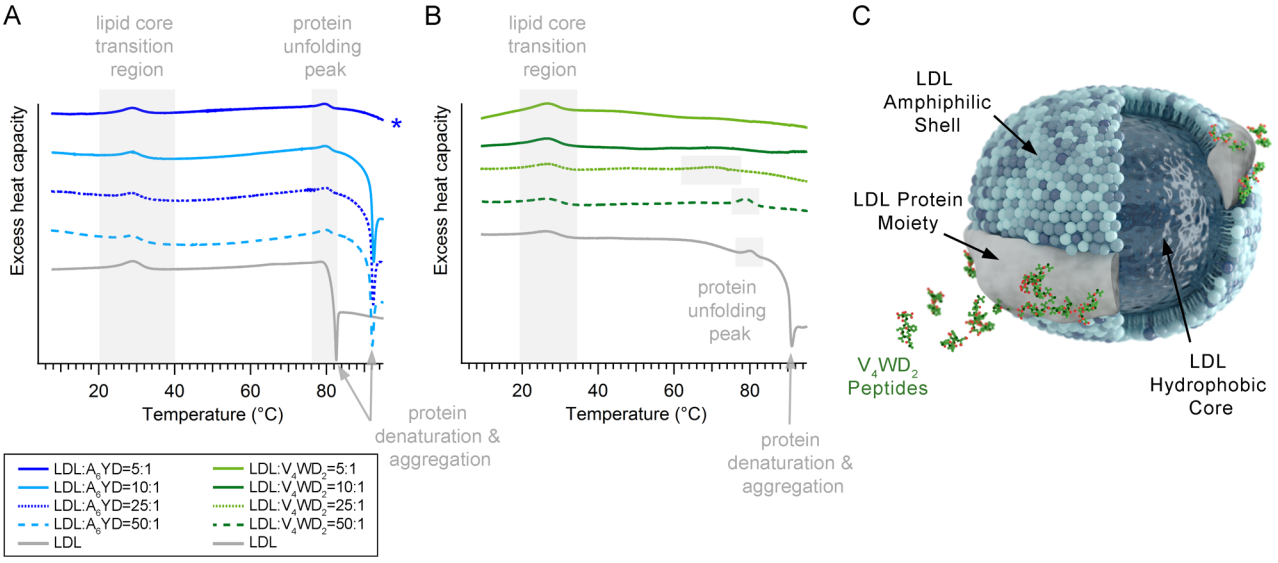

Figure 5. DSC thermograms of LDL−peptide interaction. The LDL heat capacity is plotted as a function of temperature. Samples were heated from 5 to 95 °C. The curves show a peak at ∼26−30 °C, which represents the reversible phase transition of the cholesterylester core in LDL, which was not affected by the peptides. In contrast, the transition at ∼80 °C which corresponds to protein unfolding and the subsequent exothermic reaction (which marks particle aggregation) were affected by both peptides, either in a stabilizing (A_6YD, A) or in a destabilizing way (V_4WD_2, B). All curves were shifted in the *y*-axes for clearer visibility. The asterisk marks peptide concentrations above the CAC at measurement conditions. Part C highlights the proposed V_4WD_2−LDL interaction. The peptide V_4WD_2 attaches preferably to the protein moiety of LDL. The hydrophobic core as well as the phospholipid shell remain unaffected.

assembled into extended fibers, with lengths of several hundred nanometers, whereas the fibers showed diameters of 4−10 nm with negative-staining TEM and 8−12 nm with cryo-TEM (Figure S11, and discussion on page S14). If membrane interaction is rather related to the CAC and self-assembling behavior than charge, we assume that A_6YK should be equally attracted toward the zwitterionic lipid membrane and behave similar as its negatively charged counterpart A_6YD. Indeed, also A_6YK showed no interaction with DPPC MLVs, as evidenced by DSC, EPR, and SAXS (Figure S12 and Table S4).

Interfacing Peptides with Low Density Lipoprotein (LDL). The complexity of cell membranes on the one hand and the restrictions of simple single-component phospholipid bilayers on the other hand motivated us to apply a model system that takes an "in-between" position of these two extremes. By using LDL, we aimed to investigate peptide−membrane interactions in a physiologically relevant system, with the great advantage that all constituents of the system are extremely well characterized. Human low density lipoproteins are quasi-spherical nanoassemblies with a diameter of about 22 nm.[34,35] Their physiological purpose is to carry cholesterol in human circulation. The LDL particle consists of two compartments: the lipophilic core, which is enriched in cholesterylesters and triacylglycerol, and an outer shell, composed of a phospholipid monolayer, cholesterol, and a protein component.[15] This surface heterogeneity mimics the patchiness of a cell membrane quite well. As mammalian cells, LDL particles have a net negative electrical charge[36] and the protein moiety is highly glycosylated. Due to its core−shell structure, LDL is an ideal target to study peptide-partitioning.

To figure out whether our findings from DPPC model membrane studies could be translated to LDL, we used DSC and EPR spectroscopy and tested whether peptides influenced either the lipophilic core, the amphiphilic protein−lipid shell, or both regions. As evidenced by DSC (Figure 5), LDL exhibited an endothermic transition between 26 and 30 °C, which marks the fully reversible transition of the apolar core-lipids (cholesterylesters and triacylglycerols) from a liquid-crystalline to a liquid-like phase.[16,37] This transition was not affected by the presence of A_6YD or V_4WD_2, demonstrating that peptides do not partition into the lipophilic core region of LDL. In contrast, a significant impact was observed regarding the thermotropic unfolding characteristics of the LDL protein moiety. Native LDL preparations showed an irreversible transition at around 80 °C, which is attributed to protein unfolding. This endothermic peak was followed by an exothermic reaction, which is associated with protein denaturation and aggregation. When the sample was recovered after the scan, the before clear solution had turned into cloudy precipitate. Strikingly, this exothermic reaction could be delayed in the presence of A_6YD. With increasing peptide concentrations, it was shifted to higher temperatures (Figure 5A), indicative of a stabilization of the folded protein structure. This result is in accordance with the observation of slightly increased enthalpies in DPPC MLV samples treated with the same amounts of A_6YD, also indicating stabilization (Table 2). The opposite was the case for V_4WD_2: the protein unfolding peak was shifted to lower temperatures in combination with a considerable broadening of the peak. With increased peptide concentrations, the protein unfolding peak completely vanished, suggesting that the protein already unfolded before DSC scans were conducted (Figure 5B). Considering that LDL's protein moiety is only partially embedded within the phospholipid monolayer shell, a large part including glycosylated structures is surface exposed and thus easily accessible to peptides. We therefore conclude that the protein moiety can be destabilized by direct contact with a significant fraction of molecularly available peptides (monomers and loosely connected aggregates) but not by contact with complex supramolecular structures.

To test whether peptide interaction is in fact confined to the particle surface, EPR spectroscopy was used.[38,39] As expected,

DOI: 10.1021/acs.biomac.6b01089
Biomacromolecules XXXX, XXX, XXX−XXX

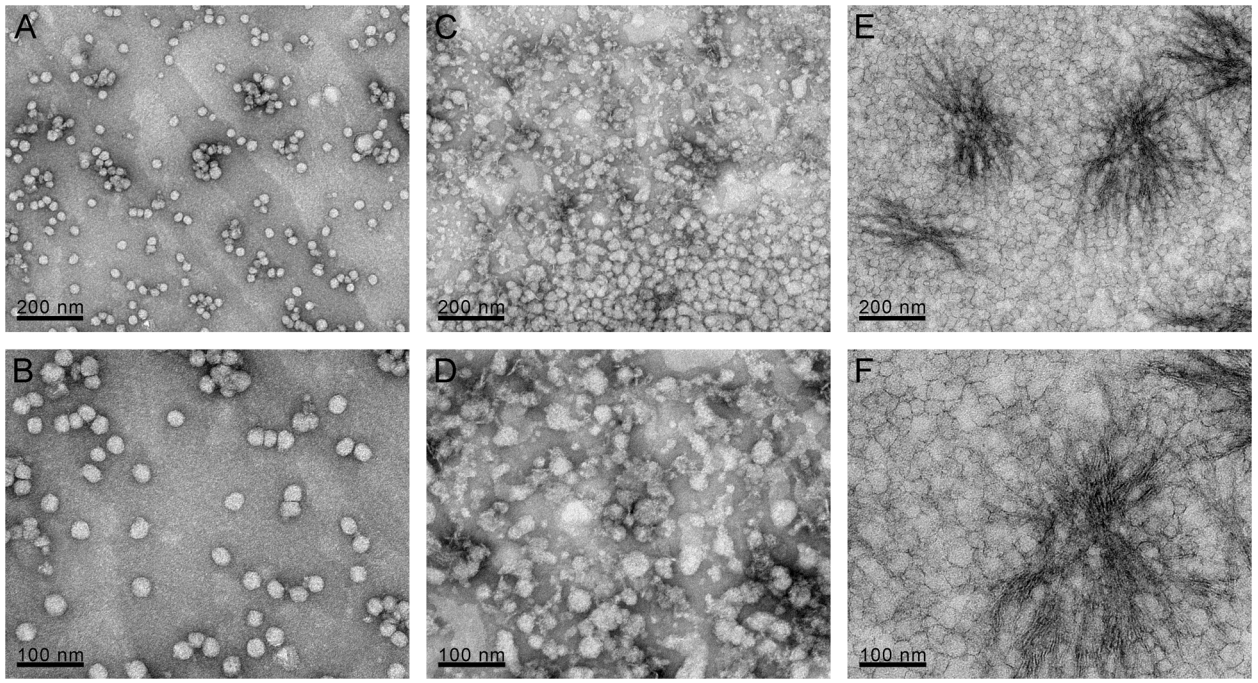

Figure 6. TEM images recorded with different magnification of native LDL (A/B), LDL in the presence of the peptides V_4WD_2 (C/D), and A_6YD (E/F). Native LDL shows well separated quasi-spherical particles (A/B). In the presence of V_4WD_2, LDL particles clustered and their morphology changed, evident by increased particle sizes, diffuse edges, and irregular shapes (C/D). In the presence of A_6YD, LDL particles were also clustered and showed a slightly changed overall morphology but were sharply confined and seemed to coexist with the self-assembled nanofibrillar peptide superstructures (E/F).

the mobility of spin probes which penetrated deeper toward the LDL core (7-MeDSA) was not affected by any peptide. Also, the surface phospholipid monolayer, probed by 5-DSA, showed no change in lipid mobility when peptides were present (see Figure S13, Tables S5 and S6). This supports our notion that peptide−LDL interaction is confined to the surface region but that V_4WD_2's activity is specifically restricted to the protein moiety of LDL. This is of particular interest, since these results comprise that V_4WD_2 affects LDL particles in a different way than proposed for DPPC MLVs. We have seen that peptides do interact with lipids when a pure lipid model membrane system is provided (such as DPPC MLVs). However, as soon as lipid−protein mixed systems are available (such as LDL), the peptides are preferentially directed toward the protein moiety and show no remarkable interaction on the lipid level. It is likely that the hydrophobic valine residues of V_4WD_2 drive this interaction and foster hydrogen-bonding interactions with the surface exposed LDL protein moiety.

Also, SAXS data on LDL did not reveal the drastic changes we might have expected when remembering the SAXS patterns of DPPC MLVs in the presence of V_4WD_2. Actually, both peptides showed the same changes in the LDL scattering patterns (Figure S14): the highest peptide concentration resulted in a slight shift of the first order maximum to lower angles, paired with a concentration dependent increased intensity at q = 0.17 nm^{-1}. An intensity increase at small angles generally indicates attractive interaction. This could be the result of peptides attaching to the LDL surface via noncovalent interactions, thus increasing the overall particle dimensions. Alternatively, the effect could also be attributed to a scattering contribution of peptide superstructures or aggregated LDL particles, or most likely a combination of all factors.

On the basis of these results, we speculate that V_4WD_2 affects LDL particles in the following way: we suggest that monomers as well as peptide aggregates attach preferably to the protein moiety of LDL, leading to strong mutual hydrogen bonding interactions (Figure 5C). In turn, the LDL protein undergoes a morphological transformation that was also indicated by a vanished DSC protein unfolding peak. In addition, hydrogen bonding between peptides and/or the protein might favor cross-linking of LDL particles, resulting in clusters or aggregation. To support this notion, we applied TEM with the aim to directly observe changes on LDL particle morphology induced by peptides. Electron micrographs of negatively stained preparations of native LDL (Figure 6A and B) showed quasi-spherical particles with diameters of approximately 19 nm. The individual particles were well separated and clearly defined by their sharp edges. The impact of V_4WD_2 on LDL particles became apparent in Figure 6C and D: throughout the images, we observed a high density of clustered LDL particles, which were irregularly sized and shaped and showed diffuse edges. However, not all LDL particles were affected. A large fraction of the population remained in its native form with slightly increased diameters of approximately 23 nm (see Figure 6C, lower part of the image). As already indicated by SAXS, we see both effects: slightly increased particle dimensions as well as LDL clustering. Arising from the distribution of native and morphologically altered LDL particles within the same sample, in combination with results obtained by SAXS and EPR, we suggest that peptide−membrane interaction shows features of cooperativity.[40−42] This means that charged peptides are not evenly distributed throughout the sample but spatially and temporally concerted. As a result, individual LDL particles are covered with peptides

DOI: 10.1021/acs.biomac.6b01089
Biomacromolecules XXXX, XXX, XXX−XXX

and thus morphologically altered, whereas others remain unattached and thus remain in their native state.

When investigating the effect of A_6YD, we got a rather different picture: LDL—although crowded and less spherical than their native counterparts—exhibited clearly defined edges (Figure 6E and F). The particles were ∼22 nm in size, and in close coexistence with the cylindrical A_6YD superstructures. Compared to assemblies of pure A_6YD, the structures appeared shorter and clustered, but their diameters remained unchanged at ∼10 nm. This finding highlights the flexible nature of peptide assembly. It shows that not only membranes adapt to the presence of peptides but also vice versa.

CONCLUSIONS

Self-assembly of amphiphilic designer peptides into supramolecular architectures is the prerequisite for using this class of molecules as materials in biomedical applications. We here present a biophysical approach to relate self-assembly propensity to membrane activity, tested on synthetic as well as biological membranes. Our results apply for two anionic amphiphilic designer peptides, with structural and chemical similarity and nonetheless different membrane-activity characteristics. In V_4WD_2, the electrostatic repulsion between the two negatively charged aspartic acid residues is dominant, so that supramolecular structure formation is inhibited for a large concentration range. This means that a large fraction of molecules is in a molecularly available state (monomers and loosely assembled aggregates). When they come into contact with membranes, we observed the following concentration-dependent effects: on a zwitterionic phospholipid bilayer model system (DPPC MLVs), electrostatic interactions most likely attract peptides to the membrane, and V_4WD_2's tryptophan residue and the high hydrophobicity of valine residues then facilitate the intercalation of the peptide into the phospholipid headgroup/interface region, thus inducing an altered membrane organization. DPPC MLVs rearrange to a system containing two different populations: pure DPPC vesicles (which were reduced in their number of layers) and lipid–peptide mixed vesicles, which show phospholipid acyl chain interdigitation. In the case of LDL, peptide monomers most probably attach to LDL's protein component, thus leading to protein unfolding, morphological alterations, and clustering of the individual particles, but maintaining the particle's lipid core integrity. In contrast, A_6YD self-assembles into highly defined cylindrical structures at concentrations >3 mM. Membrane perturbation effects are only observed at a concentration close to the CAC, or—as soon as supramolecular structures are formed—by the constant fraction of peptides that is present as monomers and small oligomers in solution (equal to the concentration of the CAC). Supramolecular peptide structures coexist with DPPC MLVs, as well as LDL particles. Depending on peptide concentration, even a stabilizing effect of A_6YD was observed on both types of model systems.

Taken together, our results indicate that membrane activity relates to the strength of intermolecular cohesive forces between peptides and thus molecular availability: peptides where large fractions are present in a molecularly dispersed state (monomers, oligomers, loose aggregates), as is the case for V_4WD_2, do interfere with membrane structures. The opposite holds for peptides that assemble into supramolecular structures at low CACs, such as A_6YD or A_6YK. These candidates seem to be well suited as potential peptide nanomaterials for regenerative medicine, drug delivery, or nanobiotechnology.

ASSOCIATED CONTENT

Supporting Information

The Supporting Information is available free of charge on the ACS Publications website at DOI: 10.1021/acs.biomac.6b01089.

HPLC and MS analysis of all peptides; concentration-dependent SAXS and ATR-FTIR measurements of A_6YD and V_4WD_2; SAXS fitting parameters of 11 mM A_6YD; additional EPR spectroscopy and SAXS data; critical evaluation of negative-staining TEM compared to cryo-TEM; fluorescence spectroscopy, TEM, SAXS, ATR-FTIR, DSC, and EPR data of A_6YK (PDF)

AUTHOR INFORMATION

Corresponding Author

*E-mail: ruth.prassl@medunigraz.at.

Author Contributions

The manuscript was written through contributions of all authors. All authors have given approval to the final version of the manuscript.

Notes

The authors declare no competing financial interest.

ACKNOWLEDGMENTS

This work has been supported by the Austrian Science Fund (FWF Project No. I 1109-N28 to R.P.). We gratefully acknowledge Ilse Letofsky-Papst from the Institute for Electron Microscopy and Nanoanalysis, Graz University of Technology and Graz Centre for Electron Microscopy for the realization of cryo-TEM experiments. We thank Elisabeth Pritz and Rudolf Schmied for their support and technical guidance with electron microscopy. We thank Georg Pabst for stimulating discussions and Hanna Lindermuth and Hans Krebs for technical assistance.

REFERENCES

(1) Aida, T.; Meijer, E. W.; Stupp, S. I. Functional supramolecular polymers. *Science* **2012**, *335* (6070), 813–7.

(2) Stephanopoulos, N.; Ortony, J. H.; Stupp, S. I. Self-assembly for the synthesis of functional biomaterials. *Acta Mater.* **2013**, *61* (3), 912–930.

(3) Boekhoven, J.; Stupp, S. I. 25th anniversary article: supramolecular materials for regenerative medicine. *Adv. Mater.* **2014**, *26* (11), 1642–59.

(4) Goktas, M.; Cinar, G.; Orujalipoor, I.; Ide, S.; Tekinay, A. B.; Guler, M. O. Self-assembled peptide amphiphile nanofibers and peg composite hydrogels as tunable ECM mimetic microenvironment. *Biomacromolecules* **2015**, *16* (4), 1247–58.

(5) Hauser, C. A. E.; Zhang, S. Designer self-assembling peptide nanofiber biological materials. *Chem. Soc. Rev.* **2010**, *39* (8), 2780–2790.

(6) Zhang, S. G. Fabrication of novel biomaterials through molecular self-assembly. *Nat. Biotechnol.* **2003**, *21* (10), 1171–1178.

(7) Zhao, X.; Pan, F.; Xu, H.; Yaseen, M.; Shan, H.; Hauser, C. A.; Zhang, S.; Lu, J. R. Molecular self-assembly and applications of designer peptide amphiphiles. *Chem. Soc. Rev.* **2010**, *39* (9), 3480–98.

(8) Kornmueller, K.; Letofsky-Papst, I.; Gradauer, K.; Mikl, C.; Cacho-Nerin, F.; Leypold, M.; Keller, W.; Leitinger, G.; Amenitsch, H.; Prassl, R. Tracking morphologies at the nanoscale: Self-assembly of an amphiphilic designer peptide into a double helix superstructure. *Nano Res.* **2015**, *8* (6), 1822–1833.

(9) Koutsopoulos, S.; Zhang, S. Long-term three-dimensional neural tissue cultures in functionalized self-assembling peptide hydrogels, Matrigel and Collagen I. *Acta Biomater.* **2013**, *9* (2), 5162–5169.

DOI: 10.1021/acs.biomac.6b01089
Biomacromolecules XXXX, XXX, XXX–XXX

(10) Wu, E. C.; Zhang, S.; Hauser, C. A. E. Self-Assembling Peptides as Cell-Interactive Scaffolds. *Adv. Funct. Mater.* **2012**, *22* (3), 456−468.
(11) Hartgerink, J. D.; Beniash, E.; Stupp, S. I. Peptide-amphiphile nanofibers: A versatile scaffold for the preparation of self-assembling materials. *Proc. Natl. Acad. Sci. U. S. A.* **2002**, *99* (8), 5133−5138.
(12) Newcomb, C. J.; Sur, S.; Ortony, J. H.; Lee, O. S.; Matson, J. B.; Boekhoven, J.; Yu, J. M.; Schatz, G. C.; Stupp, S. I. Cell death versus cell survival instructed by supramolecular cohesion of nanostructures. *Nat. Commun.* **2014**, *5*, 3321.
(13) Sommer, A.; Prenner, E.; Gorges, R.; Stutz, H.; Grillhofer, H.; Kostner, G. M.; Paltauf, F.; Hermetter, A. Organization of phosphatidylcholine and sphingomyelin in the surface monolayer of low density lipoprotein and lipoprotein(a) as determined by time-resolved fluorometry. *J. Biol. Chem.* **1992**, *267* (34), 24217−22.
(14) Lundkatz, S.; Phillips, M. C. Packing of Cholesterol Molecules in Human Low-Density-Lipoprotein. *Biochemistry* **1986**, *25* (7), 1562−1568.
(15) Prassl, R.; Laggner, P. Molecular structure of low density lipoprotein: current status and future challenges. *Eur. Biophys. J.* **2009**, *38* (2), 145−58.
(16) Deckelbaum, R. J.; Shipley, G. G.; Small, D. M.; Lees, R. S.; George, P. K. Thermal transitions in human plasma low density lipoproteins. *Science* **1975**, *190*, 392−394.
(17) Vauthey, S.; Santoso, S.; Gong, H.; Watson, N.; Zhang, S. Molecular self-assembly of surfactant-like peptides to form nanotubes and nanovesicles. *Proc. Natl. Acad. Sci. U. S. A.* **2002**, *99* (8), 5355−60.
(18) Yang, S. J.; Zhang, S. Self-assembling Behavior of Designer Lipid-like Peptides. *Supramol. Chem.* **2006**, *18* (5), 389−396.
(19) Wang, X.; Corin, K.; Baaske, P.; Wienken, C. J.; Jerabek-Willemsen, M.; Duhr, S.; Braun, D.; Zhang, S. Peptide surfactants for cell-free production of functional G protein-coupled receptors. *Proc. Natl. Acad. Sci. U. S. A.* **2011**, *108* (22), 9049−54.
(20) Koutsopoulos, S.; Kaiser, L.; Eriksson, H. M.; Zhang, S. Designer peptide surfactants stabilize diverse functional membrane proteins. *Chem. Soc. Rev.* **2012**, *41* (5), 1721−8.
(21) Fatouros, D. G.; Lamprou, D. A.; Urquhart, A. J.; Yannopoulos, S. N.; Vizirianakis, I. S.; Zhang, S.; Koutsopoulos, S. Lipid-like Self-Assembling Peptide Nanovesicles for Drug Delivery. *ACS Appl. Mater. Interfaces* **2014**, *6* (11), 8184−8189.
(22) Yau, W. M.; Wimley, W. C.; Gawrisch, K.; White, S. H. The preference of tryptophan for membrane interfaces. *Biochemistry* **1998**, *37* (42), 14713−14718.
(23) Kyte, J.; Doolittle, R. F. A simple method for displaying the hydropathic character of a protein. *J. Mol. Biol.* **1982**, *157* (1), 105−32.
(24) Amenitsch, H.; Rappolt, M.; Kriechbaum, M.; Mio, H.; Laggner, P.; Bernstorff, S. First performance assessment of the small-angle X-ray scattering beamline at ELETTRA. *J. Synchrotron Radiat.* **1998**, *5* (3), 506−508.
(25) European synchrotron radiation facility, FIT2D, http://www.esrf.eu/computing/scientific/FIT2D/ (accessed July, 2016).
(26) McConnell, H. M.; Hubbell, W. L. Molecular Motion in Spin-Labeled Phospholipids and Membranes. *J. Am. Chem. Soc.* **1971**, *93* (2), 314−326.
(27) Seelig, J. Spin Label Studies of Oriented Smectic Liquid Crystals - a Model System for Bilayer Membranes. *J. Am. Chem. Soc.* **1970**, *92* (13), 3881−3887.
(28) Seelig, J. Anisotropic Motion in Liquid Crystalline Structures. In *Spin Labeling Theory and Applications*; Berliner, L. J., Ed.; Academic Press: New York, San Francisco, London, 1976; pp 373−409.
(29) Kivelson, D. Theory of ESR Linewidths of Free Radicals. *J. Chem. Phys.* **1960**, *33* (4), 1094−1106.
(30) Mikl, C.; Peters, J.; Trapp, M.; Kornmueller, K.; Schneider, W. J.; Prassl, R. Softness of Atherogenic Lipoproteins: A Comparison of Very Low Density Lipoprotein (VLDL) and Low Density Lipoprotein (LDL) Using Elastic Incoherent Neutron Scattering (EINS). *J. Am. Chem. Soc.* **2011**, *133* (34), 13213−13215.
(31) Gofman, J. W.; Lindgren, F. T.; Elliott, H. Ultracentrifugal Studies of Lipoproteins of Human Serum. *J. Biol. Chem.* **1949**, *179* (2), 973−979.
(32) Pedersen, J. S. Analysis of small-angle scattering data from colloids and polymer solutions: modeling and least-squares fitting. *Adv. Colloid Interface Sci.* **1997**, *70*, 171−210.
(33) Nagle, J. F.; Tristram-Nagle, S. Structure of lipid bilayers. *Biochim. Biophys. Acta, Rev. Biomembr.* **2000**, *1469* (3), 159−195.
(34) Stuhrmann, H. B.; Tardieu, A.; Mateu, L.; Sardet, C.; Luzzati, V.; Aggerbeck, L.; Scanu, A. M. Neutron scattering study of human serum low density lipoprotein. *Proc. Natl. Acad. Sci. U. S. A.* **1975**, *72*, 2270−2273.
(35) Laggner, P.; Müller, K. The structure of serum lipoproteins as analysed by X-ray small-angle scattering. *Q. Rev. Biophys.* **1978**, *11* (3), 371−425.
(36) La Belle, M.; Blanche, P. J.; Krauss, R. M. Charge properties of low density lipoprotein subclasses. *J. Lipid Res.* **1997**, *38* (4), 690−700.
(37) Liu, Y.; Luo, D.; Atkinson, D. Human LDL core cholesterol ester packing: three-dimensional image reconstruction and SAXS simulation studies. *J. Lipid Res.* **2011**, *52* (2), 256−262.
(38) Kveder, M.; Pifat, G.; Pečar, S.; Schara, M. The ESR characterization of molecular mobility in the lipid surface layer of human serum lipoproteins. *Chem. Phys. Lipids* **1994**, *70* (1), 101−108.
(39) Gallova, J.; Abuja, P. M.; Pregetter, M.; Laggner, P.; Prassl, R. Site-specific effect of radical scavengers on the resistance of low density lipoprotein to copper-mediated oxidative stress: influence of alpha-tocopherol and temperature. *Chem. Phys. Lipids* **1998**, *92* (2), 139−49.
(40) Whitty, A. Cooperativity and biological complexity. *Nat. Chem. Biol.* **2008**, *4* (8), 435−439.
(41) Williamson, J. R. Cooperativity in macromolecular assembly. *Nat. Chem. Biol.* **2008**, *4* (8), 458−65.
(42) Huang, H. W. Molecular mechanism of antimicrobial peptides: The origin of cooperativity. *Biochim. Biophys. Acta, Biomembr.* **2006**, *1758* (9), 1292−1302.

DOI: 10.1021/acs.biomac.6b01089
Biomacromolecules XXXX, XXX, XXX−XXX